The 7th AOFSRR School

Cheiron School 2013

SPring-8, Japan

September 24th (Tue) – October 3rd (Thu)

~ Beamline Practice ~

BL39XU (Magnetic Materials Beamline)

1st and 2nd October 2013

Beamline scientists:

Motohiro Suzuki (JASRI/SPring-8, Leader of MCD team)
Naomi Kawamura (JASRI/SPring-8)
Masaichiro Mizumaki (JASRI/SPring-8)

Title:

Handling of X-ray polarization and application to X-ray magnetic circular dichroism spectroscopy

Abstract:

X-ray magnetic circular dichroism (XMCD) is X-ray absorption spectroscopy using circular polarized X-rays. This is a powerful technique to investigate magnetic materials, providing element specificity, electronic-shell selectivity, and angular-momentum sensitivity. XMCD experiments in the hard X-ray region (> 4 keV) require no ultra-high vacuum condition and are particularly useful to study magnetism under multiple extreme conditions (high magnetic field, low temperature, and high pressure). In the practice, you will learn how to tune several devices at the beamline, the unduator, double-crystal monochromator, and X-ray phase plate, to generate a circularly polarized X-ray beam. You will take some XMCD data by static and polarization-modulation techniques to know that how the modulation technique is useful for improving the data quality. A practice of the sum-rule analysis to determine the magnetic moments from the measured XMCD spectra will be performed.

Time Table:

09:30 – 09:45	Introduction of BL39XU
09:45 – 11:45	Controlling beamline optics (measurement of undulator spectrum and polarization using a simple polarimeter)
11:45 – 13:00	Lunch
13:00 – 14:50	X-ray magnetic circular dichroism measurement
14:50 – 15:10	Rest
15:10 – 16:45	Sum-rule analysis
16:45 – 17:00	Summary

Beamline:

BL39XU is a hard X-ray beamline covering X-ray energy of 5 – 37 keV.[1,2] Main optical components consist of the undulator, double-crystal monochromator, X-ray phase retarder, and higher-harmonics reduction mirror. Layout of the components of BL39XU is shown in figure 1.

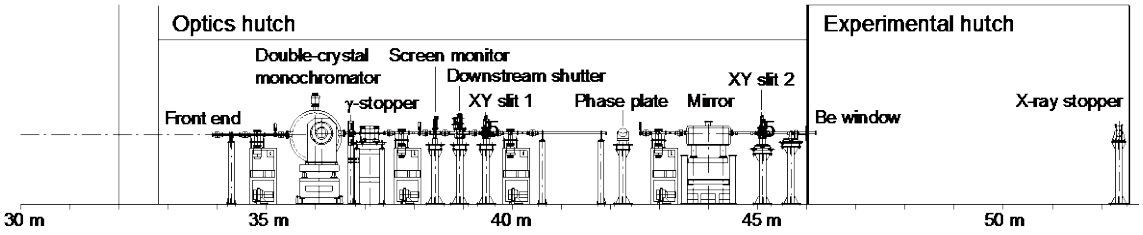

Figure 1. The layout of the optical components at BL39XU.

Undulator:

The light source of BL39XU is an in-vacuum undulator.[3] This undulator provides with extremely high-brilliance X-rays linearly polarized in the horizontal plane. The small X-ray source size and low divergence is perfectly compatible with X-ray diffractive phase retarder [4] for handling the polarization states. Table 1 summarizes the parameters of the undulator.

Table 1. BL39XU undulator source parameters.

Total length /Period /Number of period	4.5 m /32 mm /140
Minimum gap / K_{max}	8 mm /2.46
Tunable energy range (1st, 3rd and 5th)	5 – 70 keV
Peak brilliance	1.4×10^{20} photons/s/mrad^2/mm^2/0.1%b.w./100 mA
Total power /Power density	11 kW (K = 2.3) /470 kW/mrad^2
Polarization	Horizontal

Let's calculate the 1st harmonic energy of the undulator !

Photon energy of the nth-harmonic undulator radiation is given by[5]

$$E_n = 9.50 n E_B^2 \left(\lambda_u \left(1 + \frac{K^2}{2} \right) \right)^{-1} \quad \text{(eV)},$$

where,

$$K = 93.37 B_p \lambda_u$$

is a dimensionless parameter, called "deflection parameter" or "K value".

Parameters for the BL39XU undulator are:

(a) B_p = 0.820 (T) for ID gap = 8 mm

(b) B_p = 0.013 (T) for ID gap = 50 mm.

Please calculate the K value and the energy of the first harmonic E_1 for the cases (a) and (b) using values of the beam energy of the storage ring, E_B = 8 (GeV) and periodic length of the undulator, λ_u = 0.032 m.

Let's measure the undulator spectra !

The undulator spectrum depends on the gap value (also, the *K* parameter). The energy of the maximum intensity (peak energy) is changeable by changing the gap value. Here, we investigate the relationship between the gap value *G* (mm) and peak energy *E* (keV).

Gap value: *G* (mm)	Peak energy: *E* (keV)
10	
15	
20	
25	
30	

The relation of the peak energy *E* (keV) and the gap value *G* (mm) can be approximated by

$$G = -\xi \ln\left[\frac{2}{K_0^2}\left(\frac{E_{GFO}}{E} - 1\right)\right], \quad (1)$$

where ξ, K_0 and E_{GFO} are the parameters dependent on the characteristics of the undulator (period and strength of the magnets) and the electron beam energy of the storage ring. We determine these parameters by a least-square fitting of our result.

ξ (mm) =
K_0 =
E_{GFO} (keV) =

In SPring-8 users are allowed to change the undulator gap anytime, without giving any influence of the stored electron beam (independent tuning of undulator). At BL39XU the undulator gap is tuned to follow the X-ray energy determined by the monochromator at each energy point while a spectral scan. As a result, very smooth incident X-ray (I_0) spectrum is obtainable as if using a white source. This feature is important to record an EXAFS or XMCD spectrum in a wide energy range.

Let's derive the relation between ID gap and photon energy (equation (1)) !

The photon energy of the nth harmonic is described by the equation[5]

$$E_n = 9.50 n E_B^2 \left(\lambda_u \left(1 + \frac{K^2}{2} \right) \right)^{-1} \quad \text{(eV)}.$$

The dependence of the K value on the ID gap G can be approximated by $K = K_0 \exp(-c \cdot G)$.

Please derive Eq. (1) from these equations above.

Put a graph of the undulator spectrum.

Put a graph of the relation between G (mm) and E (keV).

X-ray phase retarder (XPR):

The diamond X-ray phase retarder (XPR) provides us with a freedom of the X-ray polarization: the XPR is used to convert horizontal linear polarization of the source into either circular, vertical, or elliptical polarization.[4] At BL39XU a high rate of circular polarization of $P_C > 0.9$ is achieved over the wide energy range of 5–16 keV with the use of synthetic diamond crystals of appropriate thicknesses.

Let's change the X-ray polarization !

An XPR can generate a phase-retardation between σ and π polarization components of the incident X-ray. Polarization states are controllable by changing the offset angle $\Delta\theta$ (crystal angle measured from the Bragg condition). The offset angle $\Delta\theta$ for circular ($\pm\pi/2$ retardation) or vertical polarization ($\pm\pi$ retardation) depends on the X-ray energy (wavelength), the thickness of the XPR crystal, and the reflection plane; the phase retardation δ generated by an XPR is given by [4]

$$\delta = -\frac{\pi}{2}\left[\frac{r_e^2\,\mathrm{Re}\left(F_h F_{\bar{h}}\right)}{\pi^2 V^2}\cdot\frac{\lambda^3\sin 2\theta_B}{\Delta\theta}\right]t, \qquad (2)$$

where,

* Classical electron radius $r_e = 2.8179 \times 10^{-15}$ (m)
* Crystal structure factor $\mathrm{Re}(F_h F_h) = 255.648121$ (for diamond 220 reflection)
* Unit cell volume V = 45.385 (Å^3) (for diamond crystal).

θ_B represents the Bragg angle, and t the path length of X-rays in the crystal. When $\delta = \pm\pi/2$ ($\pm\pi$) circularly (vertically) polarized X-rays are generated.

X-ray polarization state can be determined using a simple polarimeter, which consists of a Kapton scatter and two scintillation counters as shown in figure 2. When non-polarization component is negligible, the degree of linear polarization is determined by

$$P_L = \frac{I_y - I_x}{I_y + I_x}, \qquad (3)$$

where, I_y and I_x represent X-ray intensities scattered vertically and horizontally, respectively. In this case, P_L = 1, 0, and -1 means horizontally linear, circularly, and vertically linear polarization, respectively.

Here, we measure P_L at several X-ray energies using the simple polarimeter. Moreover, we determine the condition of generating circularly

and vertically polarized X-rays by analyzing our result.

Thickness of a diamond XPR: t_0 (mm) =		
E (keV)	$\Delta\theta_C$ (arcsec)	$\Delta\theta_V$ (arcsec)
6.5		
7.5		
8.5		

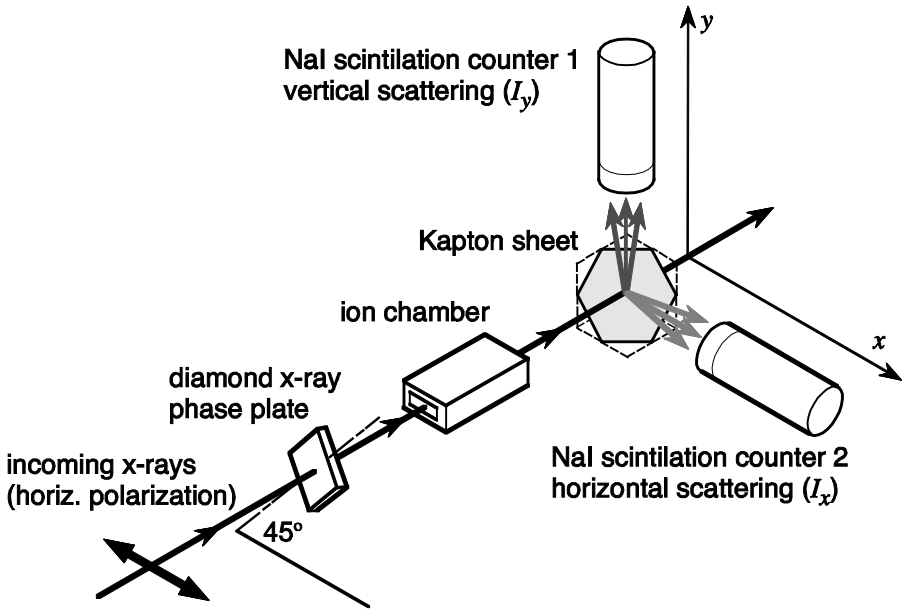

Figure 2. Configuration of the simple polarimeter system.

Put a graph of the result of XPR θ scan.

Let's calculate the optimum offset angles for vertical and circular polarizations !

Again, the phase shift δ at the offset angle $\Delta\theta$ is described by the following equation

$$\delta = -\frac{\pi}{2}\left[\frac{r_e^2\,\mathrm{Re}\left(F_h F_{\bar{h}}\right)}{\pi^2 V^2}\cdot\frac{\lambda^3\sin 2\theta_B}{\Delta\theta}\right] t \qquad (2)'.$$

Basic parameters are shown as follows:

* Classical electron radius r_e = 2.8179 × 10^{-15} (m)
* Crystal structure factor Re($F_h F_{\bar{h}}$) = 255.648121
  (for diamond 220 reflection)
* Unit cell volume V = 45.385 (Å^3) (for diamond crystal)

(a) Please confirm that the following equation can be derived from Eq. (2)':

$$\Delta\theta = -\frac{\pi}{2}\cdot\frac{1}{\delta}\cdot\lambda^3\sin 2\theta_B\cdot t\ \times\left(9.985489\times 10^{28}\right) \qquad (2)''$$

(Be careful about unit system !)

(b) Please calculate the offset angles $\Delta\theta_C$ and $\Delta\theta_V$ at which vertical ($\delta = \pi$) and circular ($\delta = \pi/2$) polarizations are respectively generated, for X-ray energies of 6.5, 7.5, and 8.5 keV.

Thickness of a diamond XPR: t_0 (mm) =		
E (keV)	$\Delta\theta_C$ (arcsec)	$\Delta\theta_V$ (arcsec)
6.5		
7.5		
8.5		

Let's derive the relation between the optimum offset angle and photon energy !

Please derive the relation between the offset angle $\Delta\theta$ allowing vertical or circular polarization and photon energy E, from Eq. (2).

X-ray magnetic circular dichroism (XMCD):

X-ray magnetic circular dichroism (XMCD) is defined as a difference in the X-ray absorption coefficients of the sample between for right- and left-circularly polarized X-rays. XMCD is a powerful tool to study the electronic and magnetic states of the ferromagnetic materials.[6, 7] In particular, its element-specific feature provides us with detailed information for the magnetic properties.[8]

The XMCD spectrometer consists of the magnet and X-ray detectors. The electromagnet and superconducting magnet are available at BL39XU. In XMCD measurement in the transmission mode, two ionization chambers are placed before and after the sample to monitor the incident (I_0) and transmitted (I) X-ray intensities. In the fluorescence mode, a Si drift detector (SDD) is usually used to monitor the fluorescence X-ray intensity from the sample, instead of the I ionization chamber. An XMCD spectrum is obtained from the X-ray absorption coefficients measured for both X-ray helicities at each energy point.

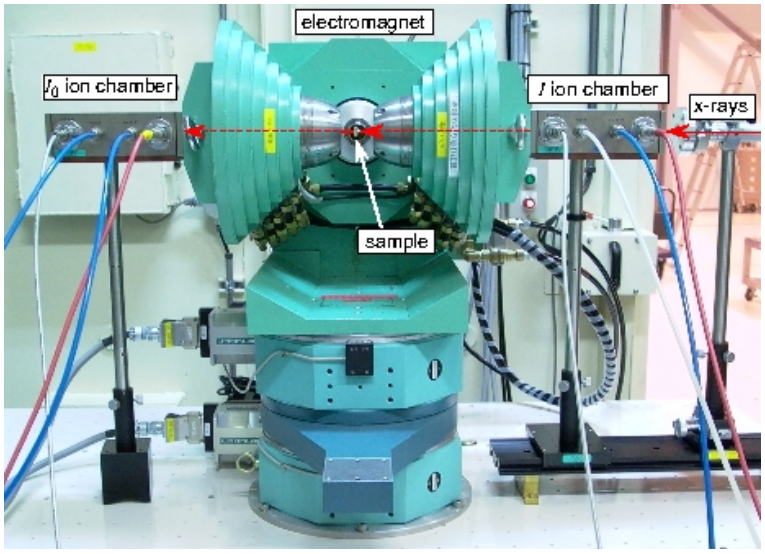

Figure 3. The XMCD spectrometer using the electromagnet.

Let's measure the XMCD spectrum !

Here, we measure XMCD spectra in $MnPt_3$ and $CoPt_3$ alloys using a helicity-reversal (static) method. If the sample shape is lump or foil, you must pay attention to the direction of the magnetic field applied so as to avoid the demagnetizing effect; magnetic field should be applied in plane for a foil sample. For fine powder samples, it does not matter which direction magnetic field is applied. The XMCD spectra are measured by the transmission-mode using two ionization chambers.

Measurement condition

Applied magnetic field: H (T)=
Sample:
Sample thickness: t (μm) =
Gain of current amplifier: I_0 @ 10 / I_1 @ 10
Energy range: E (keV) = ~
Flipping times / Counting time: / sec

Put a graph of the XMCD spectrum measured by helicity-reversal method.

Helicity-modulation XMCD measurement:

To improve the accuracy of XMCD measurement, the helicity-modulation technique [9] was developed. This technique allows a detection of dichroic signals of the order of 0.01% with a good signal-to-noise ratio. Extremely high-quality XMCD spectra are obtainable in a short acquisition time.

The helicity-modulation technique requires a combination of fast switching of the X-ray helicity and a phase-sensitive (lock-in) detection system. Block diagram of the helicity-modulation technique is shown in figure 4.

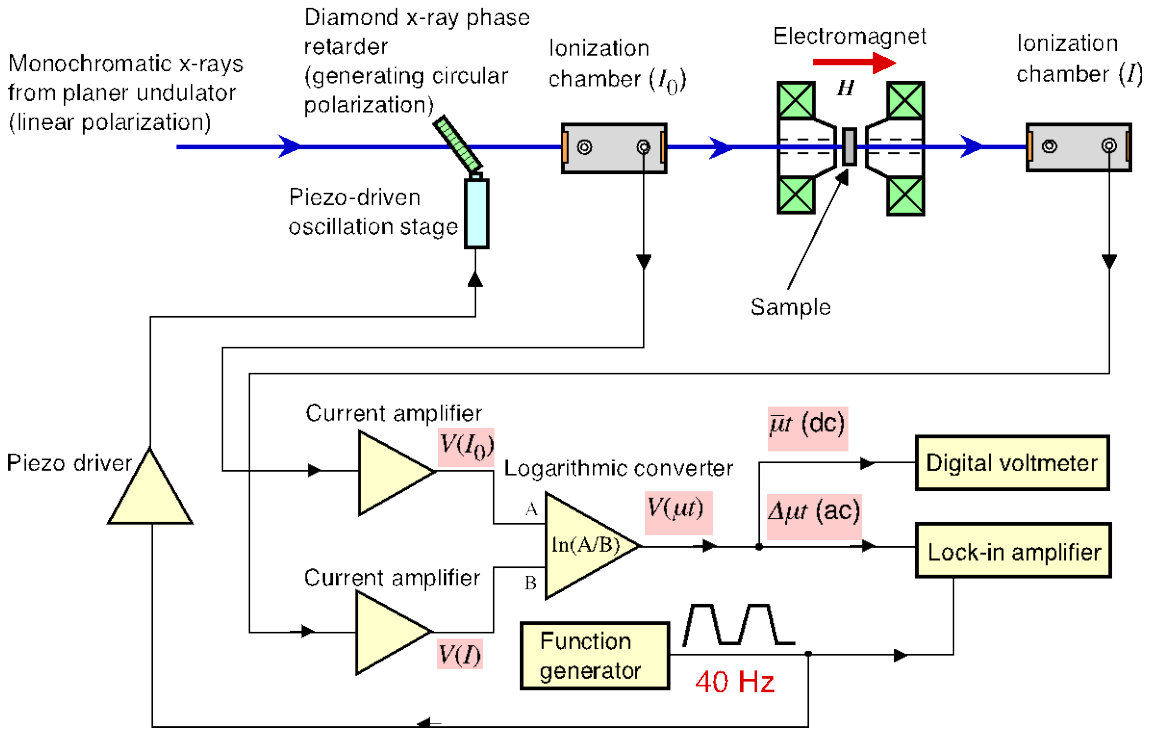

Figure 4. The block diagram of the helicity-modulation technique.

Let's experience the helicity-modulation technique !

Here, we record an XMCD spectrum of the same $MnPt_3$ and $CoPt_3$ alloys using the helicity-modulation method in the same condition of the helicity-reversal method. Then we compare the obtained spectra using the different methods, with respect to the statistic accuracy, signal-to-noise ratio, and the acquisition time.

Measurement condition

Applied magnetic field: H (T)=
Sample:
Sample thickness: t (μm) =
Gain of current amplifier: I_0 @ 10 / I_1 @ 10
Energy range: E (keV) = ~
Modulation frequency: f (Hz) =
Accumulation times:

Put a graph of the XMCD spectrum measured by helicity-modulation method.

Origin of XMCD effects:

The origin of XMCD effects is explained using a simple model for optical transitions from the 2*p* core levels to the *nd* valence states, which corresponds to the X-ray absorption at the L_2 and L_3 edges in 3*d*, 4*d*, and 5*d* transition metals. The 2*p* core levels have a large spin-orbit interaction (~10 eV for 3*d*, ~100 eV for 4*d*, and ~1 keV for 5*d* transition metals) and the core hole states are split into the $2p_{1/2}$ (L_2 edge) and $2p_{3/2}$ (L_3 edge) levels. The *nd* valence states are assumed to split into the majority and minority spin bands due to the exchange interaction, and in the following, we assume for simplicity that the majority band is fully occupied and the minority band is partially filled (i.e. there are some empty states above the Fermi energy).

Photoabsorption process basically originates from the electric dipole (E1) transition. In this case, the orbital angular momentum between the initial and final states changes by $\Delta l = l' - l = \pm 1$, and the spin angular momentum s and its magnetic quantum number m_s are conserved ($\Delta s = s' - s = 0$, $\Delta m_s = m_s' - m_s = 0$) according to the selection rules. When circular polarized X-rays with the photon helicity of $\sigma = \pm\hbar$ enters a magnetic material along the direction parallel to the magnetization, the magnetic orbital quantum number changes by $\Delta m_l = m_l' - m_l = \pm 1$. The relative transition probabilities for the $2p \rightarrow nd$ transitions can be calculated using the Clebsh-Gordan coefficients as shown in figure 5 (transition probabilities are proportional to square of the Clebsh-Gordan coefficients). According to the Fermi's golden rule, the relative transition intensity is proportional to the product of the transition probability and the density of state of the *nd* empty state. The XMCD signal, therefore, arises if imbalances in the spin or orbital density of states between major and minority bands in the final *nd* state are present.

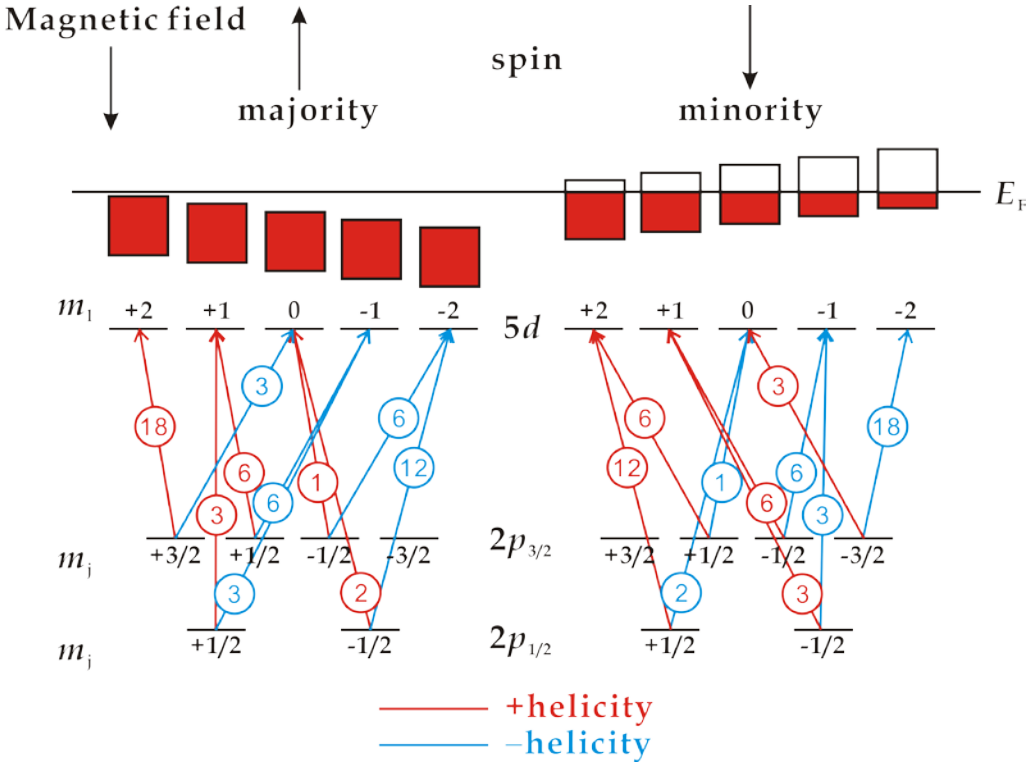

Figure 5. A simple picture of the relative transition probabilities for $2p \rightarrow 5d$ transitions. In this diagram, it is assumed that the majority spin states are completely filled.

The magneto-optical sum-rules:

P. Carra and B. T. Thole derived important formulas for XMCD spectra based on a localized model [10,11]. These formulas are called the magneto-optical sum-rules, and the expressions are described as follows:

$$\rho \equiv \frac{\int_{j_+ + j_-} d\omega\left(\mu^+ - \mu^-\right)}{\int_{j_+ + j_-} d\omega\left(\mu^+ + \mu^- + \mu^0\right)} = \frac{1}{2}\frac{l(l+1)+2-c(c+1)}{l(l+1)(4l+2-n)}\langle L_Z\rangle$$

$$\delta \equiv \frac{\int_{j_+} d\omega\left(\mu^+ - \mu^-\right) - \frac{c+1}{c}\int_{j_-} d\omega\left(\mu^+ - \mu^-\right)}{\int_{j_+ + j_-} d\omega\left(\mu^+ + \mu^- + \mu^0\right)}$$

$$= \frac{l(l+1)-2-c(c+1)}{3c(4l+2-n)}\langle S_Z\rangle + \frac{l(l+1)\left[l(l+1)+2c(c+1)+4\right]-3(c-1)^2(c+2)^2}{6lc(l+1)(4l+2-n)}\langle T_Z\rangle$$

where, μ denotes the absorption coefficient. c and l denote the orbital quantum numbers of a core hole and an excited state, respectively. $(4l + 2 - n)$ denotes the number of holes in the valence shell. The suffixes $j_\pm = c \pm 1/2$ mean the absorption edge corresponding to the core states. $\langle L_z\rangle$ and $\langle S_z\rangle$ denote the expectation values of the z component of the orbital and spin momentum operators, respectively. z is taken along the quantization axis, which is parallel to the photon wave vector. $\langle T_z\rangle$ denotes the expectation value of the magnetic dipole operator, which reflects some aspheric nature of the spin moment due either to an anisotropic charge distribution around the absorbing atom, or spin-orbit interaction.

For $2p \rightarrow nd$ transitions (corresponding to L_3 and L_2 edges), $c = 1$ ($2p$) and $l = 2$ (nd) are assigned in the equations above. Here, we define the following values, $\mu \equiv \mu^0 = (\mu^+ + \mu^-)/2$, $\Delta\mu \equiv (\mu^+ - \mu^-)$ and $n_h \equiv 4l + 2 - n$, and the following equations are obtained:

$$\rho \equiv \frac{\int_{L_3+L_2} (\Delta\mu)d\omega}{\int_{L_3+L_2} (\mu)d\omega} = \frac{3}{2n_h}\langle L_Z\rangle$$

$$\delta \equiv \frac{\int_{L_3} (\Delta\mu)d\omega - 2\int_{L_2} (\Delta\mu)d\omega}{\int_{L_3+L_2} (\mu)d\omega} = \frac{1}{n_h}\left(2\langle S_Z\rangle + 7\langle T_Z\rangle\right)$$

These formulas allow us to calculate the value of the orbital angular momentum $\langle L_z\rangle$ and the spin angular momentum $\langle S_z\rangle$ separately from the

experimental results. Basically, the value of $\langle T_z \rangle$ term is smaller than the $\langle S_z \rangle$ term in most practical cases, in which the spin-orbit coupling in the final *nd* states are negligibly small. However, $\langle T_z \rangle$ value is not always negligible compared to $\langle S_z \rangle$ in case of low crystal symmetry [12,13]. In case of the sample with a cubic symmetry, $\langle T_z \rangle$ value is negligible [14]. Application of sum-rules is one of the most useful tools provided by XMCD spectroscopy.

Let's apply the sum-rules to the experimental results !

Here, we apply the sum-rules to the experimental results for Pt in $MnPt_3$ and $CoPt_3$, and obtain $\langle L_z \rangle$ and $\langle S_z \rangle$ values. The required values to obtain $\langle L_z \rangle$ and $\langle S_z \rangle$ are integrals of the white-line parts at the $L_{3,2}$ edges, integrals of the XMCD profiles at the $L_{3,2}$ edges, and the number of holes, n_h. All the values except for n_h can be determined experimentally. There are several ways to obtain the white-line integrals: (1) to assume a background function (transition to continuous levels), for example, an arctangent function, a step function, etc., (2) to use an experimental XAS spectrum in a full-filled *d*-level material such as Au or materials including Au atoms. For n_h, literature values reported by band calculations are often used. The orbital and spin magnetic moments are given by the relations, $m_L = -\mu_B \langle L_z \rangle$ and $m_S = -2\mu_B \langle S_z \rangle$, where μ_B denotes the Bohr magneton. Finally, you obtain the orbital and spin magnetic moments of the target Pt atoms in $MnPt_3$ and $CoPt_3$.

Sum-rule analysis: n_h =				$\langle T_z \rangle$ =			
Material	$\langle L_z \rangle / \langle S_z \rangle$	$\langle L_z \rangle$	m_L (μ_B)	$\langle S_z \rangle$	m_S (μ_B)	$m_L + m_S$ (μ_B)	Ref. (μ_B)
$MnPt_3$							0.26 [16]
$CoPt_3$							0.26 [17]

References:

[1] See URL: http://www.spring8.or.jp/en/users/current_user/bl/beamline/BLtable/

[2] H. Maruyama *et al.*: J. Synchrotron Rad. **6** (1999) 1133.

[3] T. Hara *et al.*: J. Synchrotron Rad. **5** (1998) 403.

[4] K. Hirano and H. Maruyama: Jpn. J. Appl. Phys. **36** (1997) L1272.

[5] H. Kitamura, J. Synchrotron Rad. **7** (2000) 121.

[6] N. Ishimatsu *et al.*: J. Phys. Soc. Jpn. **76** (2007) 064703.

[7] N. Kawamura *et al.*: J. Phys. Soc. Jpn. **76** (2007) 074716.

[8] A good example is given in : A. Koizumi *et al.*: Phys. Rev. **B61** (2000) R14909.

[9] M. Suzuki *et al.*: Jpn. J. Appl. Phys. **37** (1998) L1488.

[10] B. T. Thole *et al.*, Phys. Rev. Lett. **68** (1992) 1943.

[11] P. Carra *et al.*, Phys. Rev. Lett. **70** (1993) 694.

[12] J. Vogel *et al.*, Phys. Rev. **B55** (1997) 3663.

[13] W. Grange *et al.*, Phys. Rev. **B58** (1998) 6298.

[14] R. Wu and A. J. Freeman, Phys. Rev. Lett. **73** (1994) 1994.

[15] W. Grange *et al.*, Phys. Rev. **B58** (1998) 6298.

[16] B. Antonini *et al.*, Phys. Rev. **187** (1969) 611.

[17] F. Menzinger and A. Paoletti, Phys. Rev. **143** (1966) 365.